

# From Pairs to Sequences: Track-Aware Policy Gradients for Keypoint Detection

Yepeng Liu<sup>1\*</sup>, Hao Li<sup>2\*</sup>, Liwen Yang<sup>1\*</sup>, Fangzhen Li<sup>2†</sup>, Xudi Ge<sup>1</sup>, Yuliang Gu<sup>1</sup>,  
Kuang Gao<sup>2</sup>, Bing Wang<sup>2</sup>, Guang Chen<sup>2</sup>, Hangjun Ye<sup>2</sup>, Yongchao Xu<sup>1†✉</sup>

<sup>1</sup>School of Computer Science, Wuhan University <sup>2</sup>Xiaomi EV

{yepeng.liu@, liwenyang@, yongchao.xu@}whu.edu

## Abstract

Keypoint-based matching is a fundamental component of modern 3D vision systems, such as Structure-from-Motion (SfM) and SLAM. Most existing learning-based methods are trained on image pairs, a paradigm that fails to explicitly optimize for the long-term trackability of keypoints across sequences under challenging viewpoint and illumination changes. In this paper, we reframe keypoint detection as a sequential decision-making problem. We introduce **TraqPoint**, a novel, end-to-end Reinforcement Learning (RL) framework designed to optimize the **Track-quality** (Traq) of keypoints directly on image sequences. Our core innovation is a track-aware reward mechanism that jointly encourages the consistency and distinctiveness of keypoints across multiple views, guided by a policy gradient method. Extensive evaluations on sparse matching benchmarks, including relative pose estimation and 3D reconstruction, demonstrate that TraqPoint significantly outperforms some state-of-the-art (SOTA) keypoint detection and description methods.

## 1. Introduction

Keypoint detection and description are the foundation for a wide range of 3D computer vision tasks, including Structure-from-Motion (SfM) [25, 43], Simultaneous Localization and Mapping (SLAM) [6, 29], and relocalization [39, 53]. The performance of these systems is critically dependent on the quality of the detected keypoints. To enable robust matching, these points must exhibit high stability under drastic viewpoint and illumination changes.

Driven by advances in deep learning, the paradigm for keypoint detection has progressively shifted from hand-crafted designs to data-driven approaches. These learning-based methods are generally self-supervised or supervised. Self-supervised methods, such as SuperPoint [9] and SiLK [15], generate pseudo-labels from synthetic image pairs using geometric transformations. Supervised approaches [5, 11, 50, 55] instead train on large-scale real-

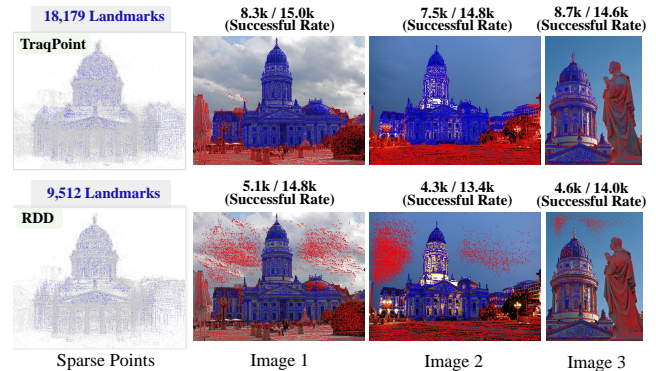


Figure 1. Multi-view reconstruction: Our TraqPoint vs. RDD [5]. Keypoints that successfully generate landmarks are marked in blue. Failed keypoints are marked in red. Our TraqPoint generates more keypoints in structurally significant areas with higher cross-view consistency, yielding more landmarks.

world datasets (e.g., MegaDepth [23]) to learn repeatable keypoints. Another category of methods (RFP [3], DISK [48], and RIPE [19]) proposes using Reinforcement Learning (RL) to select keypoints in a pair of images, rewarding those keypoints that can form matching pairs. Despite their varied training strategies, existing methods converge on a common principle: defining keypoint quality through its repeatability and matchability in an image pair.

This pairwise training paradigm has significantly improved performance on matching tasks. However, it inherently optimizes for instantaneous “matchability” within isolated image pairs. This objective is misaligned with sequential applications (e.g., SLAM and SfM), where the core requirement is long-term “trackability”. Specifically, keypoints that perform well on a single pair may drift or drop over long trajectories due to strong viewpoint/illumination changes or motion blur. Such failures directly compromise the stability and accuracy of the overall system.

In this paper, we advocate for a paradigm shift: moving from optimizing “pairwise matchability” to directly learning for “long-term trackability”. To this end, we introduce a novel **Sequence-Aware Keypoint Policy Learning**

\* Equal contribution, † Project leader, ✉ Corresponding author.

framework. We reframe keypoint detection as a sequential decision-making problem, where the goal is to discover points that yield stable and persistent tracks. In our framework, a policy network acts as a RL agent that operates on a single reference image to select a sparse set of candidate keypoints. The “environment” is no longer a single paired image but an entire sequence. Correspondingly, the reward is a function of the quality of the entire track generated by each selected keypoint.

Specifically, the reward for a track is a composite of two signals: (1) a **Rank Reward** that incentivizes selecting points maintaining high saliency within their local neighborhood across multiple views, and (2) a **Distinctiveness Reward** that encourages selecting points with global uniqueness. By optimizing this track-centric objective, our policy network learns to produce a detection probability map that intrinsically favors points with the highest potential for long-term stability. As shown in Fig. 1, TraqPoint’s keypoints are concentrated in structurally significant areas and exhibit superior cross-view consistency compared to the state-of-the-art approach, RDD [5]. Extensive experiments confirm that TraqPoint achieves SOTA results—specifically on both pairwise and sequential downstream tasks, including relative pose estimation, visual localization, visual odometry, and 3D reconstruction.

Our main contributions can be summarized as follows:

- We identify a critical gap between the pairwise training paradigm and the demands of sequential applications. To bridge this gap, we pivot to a new perspective and propose a novel Reinforcement Learning (RL) framework that directly optimizes long-term keypoint trackability.
- For the RL framework, we propose a hybrid sampling strategy that enables efficient candidate keypoint selection, while also introducing a novel composite reward function to jointly optimize for multi-view consistency and distinctiveness.
- Through comprehensive experiments, we show that TraqPoint significantly outperforms state-of-the-art methods on both pairwise tasks and sequential tasks.

## 2. Related Work

### 2.1. Learned Keypoint Detection and Description

The definition of a “good” keypoint has evolved from classical handcrafted [26, 28, 35, 36, 52] designs to modern learning-based paradigms [2, 18, 20, 31, 34, 38, 42]. Traditional algorithms defined core properties of desirable keypoints: SIFT [26] identifies scale-space extrema via Difference-of-Gaussians, valuing scale stability and rotation invariance; FAST [35] and ORB [36] prioritize efficiency, detecting corners via surrounding pixel intensities. TBMR [52] leverages Morse theory for keypoint extraction, emphasizing contrast and affine invariance. These methods share the principle that ideal keypoints lie in textured

regions with strong, repeatable geometric signatures (*e.g.*, corners, blobs).

The learning-based paradigm has dramatically improved the robustness of keypoint detection and matching in complex scenes through a data-driven, pairwise training approach. One line of work uses self-supervision, typically by leveraging homography transformations to generate image pairs with known correspondences. SuperPoint [9], for example, uses a base detector to create pseudo-labels on warped images, enabling joint training of the detector and descriptor. Similarly, R2D2 [34] optimizes for both repeatability and reliability in a self-supervised manner, while SILK [15] uses the matchability of learned descriptors to supervise which points should be detected. Another category of methods, including D2-Net [10], ALIKED [55], XFeat [33], DeDoDe [11], and RDD [5], trains on large-scale 3D datasets like MegaDepth [23]. By using ground-truth correspondences derived from COLMAP [43] reconstructions, these methods learn features that are highly consistent across real-world viewpoint and illumination changes. Furthermore, dense (RoMa [12], Mast3r [21], Dust3r [49]) and semi-dense (LoFTR [46], Efficient LoFTR [51]) matching methods have garnered significant attention recently, and they also adopt a pairwise training paradigm.

While these methods have established a strong baseline for pairwise matching, their objective is not explicitly designed to model long-term temporal dynamics. Our work addresses this gap by introducing a sequence-aware paradigm that optimizes directly for long-term trackability. This approach offers greater potential to handle complex factors inherent in sequences.

### 2.2. RL-Based Keypoint Detection

Several works frame keypoint detection as a Reinforcement Learning (RL) problem to handle the discrete and non-differentiable keypoint selection task. Early approaches, such as [7, 47], utilize Q-learning to directly regress a keypoint’s reward value. However, these rewards are calculated based on the matchability of handcrafted descriptors (*e.g.*, SIFT), which fundamentally limits the robustness of the learned detector.

More recent methods [3, 13, 19, 32, 37, 48] perform gradient optimization directly in policy space. Reinforced Feature Points (RFP) [3] represents a key advancement by embedding the learning process into high-level tasks, using the final pose estimation error as the reward signal to align keypoint selection with 3D geometry. DISK [48] achieves end-to-end optimization by using the number of geometrically consistent inliers as a reward, while RIPE [19] proposes an unsupervised approach that uses the inlier ratio from epipolar constraints. These methods still retain the limitation of the pairwise paradigm: their reward functions

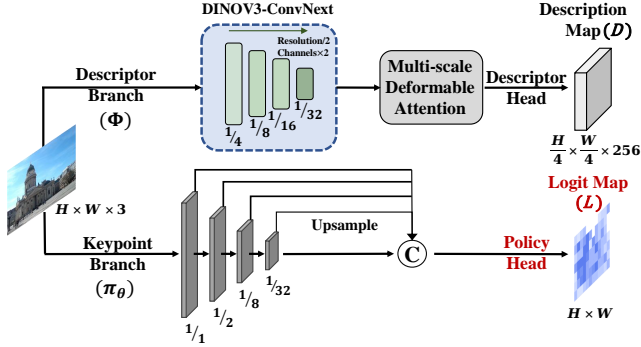


Figure 2. Following the architectural design of RDD [5], we adopt an identical network structure. Specifically, we replace the feature extractor employed in RDD [5] with DINOv3-ConvNeXt [45]. The keypoint branch serves as the **policy network** ( $\pi_\theta$ ).

are derived from a single image pair, optimizing for instantaneous matchability rather than the longevity of keypoints required in sequential tasks.

Our work departs from these RL-based methods by shifting the optimization paradigm from pairwise to sequence-level supervision, computing rewards based on the trajectory quality of selected keypoints to directly optimize for “trackability” over “matchability”. Furthermore, we decouple policy learning from descriptor training, leveraging a frozen descriptors branch to provide stable reward signal.

### 3. Method

Our TraqPoint utilizes a lightweight policy network and a sequence-aware reward to select keypoints explicitly optimized for long-term trackability. In Section 3.1, we first introduce the preliminaries, detailing the dual-branch network architecture (Fig. 2) and the pre-training of the descriptor branch, which provides a stable signal for reward calculation. Subsequently, we formally define the Problem Formulation (Sec. 3.2) of our RL approach. We then detail our core innovations: hybrid sampling strategy (Sec. 3.3) and the trackability reward (Sec. 3.4). Finally, we describe the policy optimization process (Sec. 3.5) for the network. Fig. 3 illustrates the complete RL training process.

#### 3.1. Preliminaries

Our method builds upon the recent success of dual-branch architectures [5, 11]. We adopt a “describe-then-detect” training paradigm, where the descriptor branch is pre-trained first and then kept frozen in keypoint branch training. This two-stage strategy allows our framework to focus exclusively on optimizing the keypoint detection policy, which is the core of our work.

**Network Architecture.** As shown in Fig. 2, we adopt the same network architecture as RDD [5]. The descriptor branch consists of a backbone and a multi-scale deformable

transformer module. We replace the original ResNet-50 backbone with a DINOv3-ConvNeXt (base) [45] and utilize its features from four different scales. The transformer module then aggregates these features to produce a dense descriptor map  $D \in \mathbb{R}^{\frac{H}{4} \times \frac{W}{4} \times 256}$ . The keypoint branch retains the lightweight 4-layer convolutional design from ALIKED [55]. As this branch serves as the policy network in our RL framework, we term its final  $1 \times 1$  convolutional layer the policy head, which outputs the final logit map  $L \in \mathbb{R}^{H \times W}$ .

While this backbone upgrade improves performance (see ablation in Sec. 4.7), our primary contribution is the novel RL training paradigm, not the architectural modifications.

**Descriptor Branch Pre-training.** Following prior work [5, 33], we train the descriptor branch  $\Phi$  on image pairs from the MegaDepth dataset [23]. We first leverage camera poses and depth maps to generate ground-truth pixel correspondences  $\mathcal{M}_{\text{gt}}$ . For a given pair  $(I_A, I_B)$ , we sample the corresponding sets of descriptors  $\mathbf{d}_A$  and  $\mathbf{d}_B$  from the outputs of  $\Phi$ . We then compute the similarity matrix  $\mathbf{S}$  between  $\mathbf{d}_A$  and  $\mathbf{d}_B$ , and apply a dual-softmax operation to obtain the probability matrix  $\mathbf{P}$ . To optimize the network, we apply the same focal loss function [5] on the positive correspondences (diagonal elements  $\mathbf{P}_{ii}$ ):

$$\mathcal{L}_{desc} = -\frac{1}{|\mathcal{M}_{\text{gt}}|} \sum_{i \in \mathcal{M}_{\text{gt}}} \alpha (1 - \mathbf{P}_{ii})^\gamma \log(\mathbf{P}_{ii}), \quad (1)$$

where  $\alpha = 0.25$  and  $\gamma = 2$ . Upon completion of this training stage, we freeze the parameters of  $\Phi$ .

#### 3.2. Problem Setup

To address the dual challenges of the discrete selection problem inherent in keypoint detection and the objective misalignment of pairwise training, we introduce a reinforcement learning framework that reformulates keypoint detection as a sequential decision-making task. In this framework, the policy network  $\pi_\theta$  (parameterized by  $\theta$ ) acts as the agent. The state  $s$  is defined as the reference image  $I^{ref}$ . Given  $s$ , the policy outputs a pixel-wise probability distribution, denoted as  $P_\theta = \pi_\theta(s)$ , over the image spatial domain. An action is defined as sampling a set of  $N$  keypoints independently from this distribution:  $\mathcal{A} = \{\mathbf{x}_i\}_{i=1}^N$ , where  $\mathbf{x}_i \sim P_\theta$ . The objective is to maximize the expected reward  $\mathcal{R}(\mathcal{A})$ , which is the average long-term trackability score  $R_i$  for each keypoint in  $\mathcal{A}$  (detailed in Sec. 3.4). This is formulated as maximizing the objective function:

$$\mathcal{J}(\theta) = \mathbb{E}_{\mathcal{A} \sim P_\theta} [\mathcal{R}(\mathcal{A})]. \quad (2)$$

#### 3.3. Hybrid Sampling Strategy

While the action set  $\mathcal{A}$  is sampled from the policy’s output distribution  $P_\theta$ , the specific sampling method significantly impacts performance. A naive approach of sampling

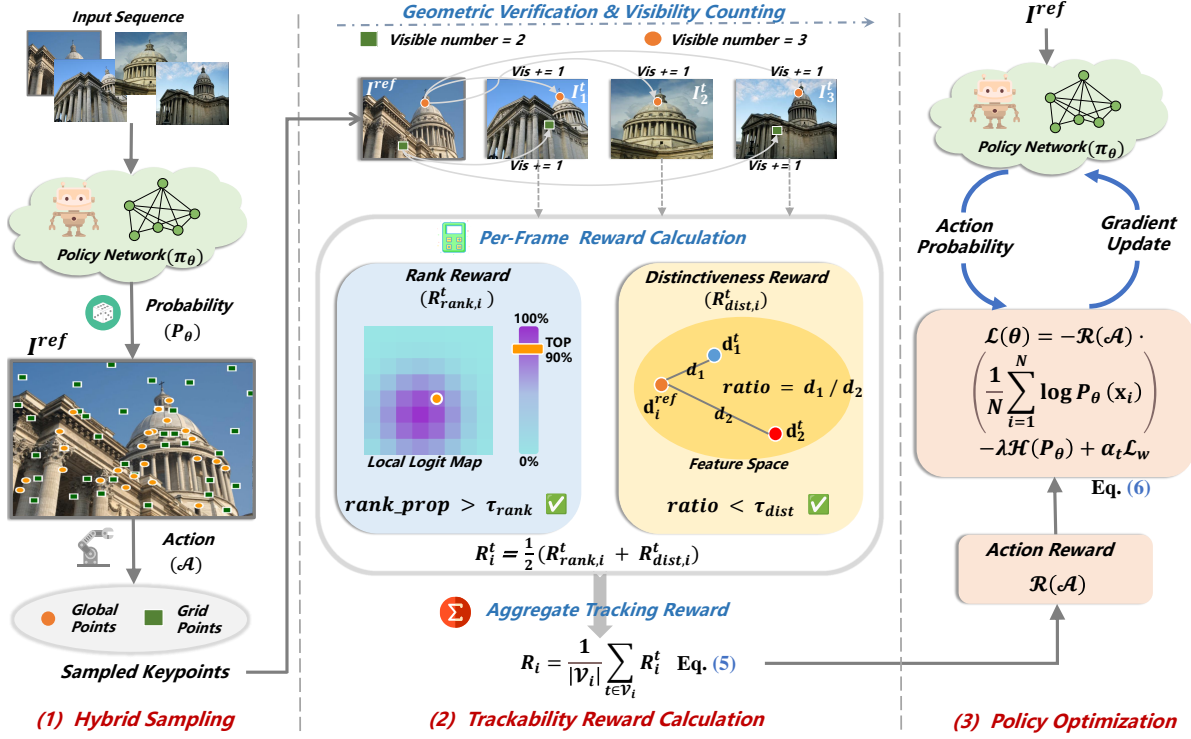


Figure 3. Overview of our proposed Sequence-Aware Keypoint Policy Learning framework: First, we select a reference frame from the input image sequence and perform hybrid keypoint sampling on it. Next, we leverage geometric mapping to locate the corresponding positions of the reference frame’s keypoints in other frames of the sequence. We then count the number of these keypoints visible across the entire sequence. After that, we compute per-frame rewards for each sampled point and aggregate these into a final track reward. Finally, we update the policy network’s gradients.

from the global distribution can cause keypoints to cluster in high-probability regions, resulting in poor spatial coverage. We therefore propose a hybrid sampling strategy to balance exploitation and exploration (via spatial coverage). Specifically,  $\mathcal{A}$  is a union of two subsets:

- **Global Sampling:** We sample  $N_g$  points by drawing directly from the global distribution  $P_\theta$ , focusing on high-probability regions.
- **Grid Sampling:** We divide the image into a  $G \times G$  regular grid (resulting in  $N_{\text{grid}} = G^2$ ). For each cell, we first extract the local logit submap from  $L$  and apply spatial softmax to obtain a local policy distribution. We then sample one keypoint from each cell based on this local distribution, ensuring spatial coverage while selecting locally optimal points.

This hybrid approach generates a spatially diverse set of  $N = N_g + N_{\text{grid}}$  keypoints. For the policy gradient calculation, the probability of every sampled keypoint  $\mathbf{x}_i \in \mathcal{A}$  (regardless of its source) is defined by its value in the global distribution  $P_\theta(\mathbf{x}_i)$ .

### 3.4. Trackability Reward Formulation

The core of our framework is the reward function  $R_i$  for each sampled keypoint  $\mathbf{x}_i \in \mathcal{A}$  (located in  $I^{\text{ref}}$ ). For each keypoint  $\mathbf{x}_i$ , we project it into every target frame  $I^t$  using

the known relative pose and depth, yielding a projected coordinate  $\mathbf{x}_i^t$ . A projection is considered visible if it falls within the image bounds and passes standard geometric verification checks (such as depth consistency). We denote the set of frame indices  $t$  where  $\mathbf{x}_i$  is visible as  $\mathcal{V}_i$ .

For each visible projection  $\mathbf{x}_i^t$  (where  $t \in \mathcal{V}_i$ ), we compute a per-frame reward  $R_i^t$ . To prevent sparse signals, both components of this reward are designed as linear scores rather than binary pass/fail signals. This  $R_i^t$  combines two complementary signals:

**Rank Reward ( $R_{\text{rank}}$ ).** This reward quantifies the cross-view consistency of saliency for high-probability points selected from the  $I^{\text{ref}}$ . In the target frame  $I^t$ , we compute the logit map  $L^t = \pi_\theta(I^t)$ . We assess the logit value  $L^t(\mathbf{x}_i^t)$  relative to its local  $K \times K$  patch. We define `rank_prop` as the saliency percentile score, representing the proportion of points it is more salient than. For example, in a  $10 \times 10$  patch (100 points), the 10th-highest logit value has a `rank_prop` of 0.9 (as it is more salient than 90% of the points). We set a cutoff threshold  $\tau_{\text{rank}} = 0.2$ , meaning only points that are more salient than the bottom 20% of points receive a reward. This reward is defined as follows:

$$R_{\text{rank},i}^t = \max\left(0, \frac{\text{rank\_prop} - \tau_{\text{rank}}}{1.0 - \tau_{\text{rank}}}\right). \quad (3)$$

**Distinctiveness Reward ( $R_{\text{dist}}$ ).** This reward, inspired by Lowe’s ratio test [26], measures the distinctiveness of the selected point. We use the frozen descriptor branch  $\Phi$  to get the reference descriptor  $\mathbf{d}_i = \Phi(I^{\text{ref}}, \mathbf{x}_i)$ . We then compare  $\mathbf{d}_i$  against the set of all  $N$  projected descriptors in the target frame,  $\{\mathbf{d}_j^t = \Phi(I^t, \mathbf{x}_j^t) \mid j = 1 \dots N \text{ and } t \in \mathcal{V}_j\}$ . Let  $d_1$  and  $d_2$  be the distances to the nearest and second-nearest neighbors of  $\mathbf{d}_i$  within this set of  $N$  descriptors. We define  $\text{ratio} = d_1/d_2$ . We reward points only if this ratio is below our threshold  $\tau_{\text{dist}} = 0.85$ . This reward is linearly scaled:

$$R_{\text{dist},i}^t = \max\left(0, \frac{\tau_{\text{dist}} - \text{ratio}}{\tau_{\text{dist}}}\right). \quad (4)$$

The per-frame reward  $R_i^t$  is the average of these two components. The final trackability reward for keypoint  $\mathbf{x}_i$  is  $R_i$ :

$$R_i = \frac{1}{|\mathcal{V}_i|} \sum_{t \in \mathcal{V}_i} R_i^t. \quad (5)$$

If a keypoint is never visible ( $|\mathcal{V}_i| = 0$ ), its reward  $R_i$  is zero.

### 3.5. Policy Optimization

We optimize the policy network  $\pi_\theta$  using a composite loss function. The primary component is the policy gradient term. To reduce variance, we use the average reward of the entire action set. Let  $\mathcal{R}(\mathcal{A}) = \frac{1}{N} \sum_{i=1}^N R_i$ . The policy gradient is then estimated using the average log-probability of all sampled actions,  $\log P_\theta(\mathbf{x}_i)$  (from Sec. 3.3). Second, to encourage spatial diversity and prevent mode collapse, we add a spatial entropy regularization term,  $\mathcal{H}(P_\theta) = -\sum_{\mathbf{x}} P_\theta(\mathbf{x}) \log P_\theta(\mathbf{x})$ . Finally, to accelerate convergence in the early stages, we employ a warm-up loss  $\mathcal{L}_w$  for the initial 10% of training epochs. This term uses keypoint locations from the FAST detector [35] to weakly supervise the sigmoid of the policy’s logit map (*e.g.*, via a BCE loss). The final loss function is:

$$\mathcal{L}(\theta) = -\mathcal{R}(\mathcal{A}) \cdot \left( \frac{1}{N} \sum_{i=1}^N \log P_\theta(\mathbf{x}_i) \right) - \lambda \mathcal{H}(P_\theta) + \alpha_t \mathcal{L}_w, \quad (6)$$

where  $\lambda$  is a fixed hyperparameter that balances the entropy term with the main loss, and is set to 0.001. The warm-up weight  $\alpha_t$  linearly anneals from 1.0 to 0.0 during the first 10% of epochs, after which only the RL loss remains.

## 4. Experiments

To fully validate the effectiveness of our proposed TraqPoint, we conduct evaluations on pair-level tasks (relative pose estimation, visual localization), and sequence-level tasks (visual odometry, 3D reconstruction). Furthermore, we perform ablation experiments to dissect the contributions of the key modules in our framework.

### 4.1. Training Data

We construct sequential training data from the MegaDepth dataset [23] for keypoint branch training. Specifically, we first randomly select a reference image from each sub-scene, then identify the remaining images that have an overlap ratio between 10% and 70% with the reference via their depth maps and camera poses, and finally randomly sample images from this overlapping subset to form a training sequence with the reference. Additional details about the data construction are provided in the supplementary material.

### 4.2. Implementation Details

For descriptor pre-training, images are resized to 800px. For keypoint policy learning, images are resized to 480px, and we use fixed-length sequences of 5 images with  $N = 256$  keypoints sampled per RL step. Both stages are trained for 50,000 steps on 8 NVIDIA H20 GPUs. We use Adam optimizer with a cosine annealing learning rate scheduled from  $2 \times 10^{-4}$  down to  $5 \times 10^{-6}$ . During inference, we apply a sigmoid function to the output of keypoint branch and use Non-Maximum Suppression (NMS) with a  $5 \times 5$  window to extract keypoints. Following [5, 48], we utilize the soft mutual nearest neighbor (MNN) operation, which computes matching probabilities by applying softmax over both dimensions of the descriptor similarity matrix. We discard matches with probability below 0.01 for feature matching. A comparison of the runtime between our method and other approaches is provided in the supplementary material.

### 4.3. Relative Pose Estimation

**Datasets.** Following prior works [5, 33], we use the MegaDepth [23] and ScanNet [8] test sets to evaluate the relative pose estimation task. These datasets feature outdoor and indoor scenes respectively, and their main challenges include large viewpoint changes, illumination variations, and repetitive textures. There is no overlap between these test sets and our training set.

**Metrics and Compared Methods.** We report the Area Under the Curve (AUC) for pose errors at thresholds of  $5^\circ$ ,  $10^\circ$ , and  $20^\circ$ . To ensure reliable pose estimation, we use the RANSAC function of OpenCV [4] to solve for the essential matrix. We compared TraqPoint against the state-of-the-art detector/descriptor methods [5, 9, 11, 19, 33, 48, 55], and learned matching methods [24, 40]. For all methods, images are resized to a maximum dimension of 1,600 pixels for the MegaDepth dataset, while the VGA resolution is used for the ScanNet dataset. All methods sample the top-4096 keypoints, and conduct experiments following the optimal settings from their official repositories.

**Results.** Tab. 1 shows our TraqPoint outperforms some state-of-the-art pairwise and RL-based methods across the MegaDepth and ScanNet benchmarks. Specifically, compared to RDD [5], we improve the AUC@5 by 3.9 and

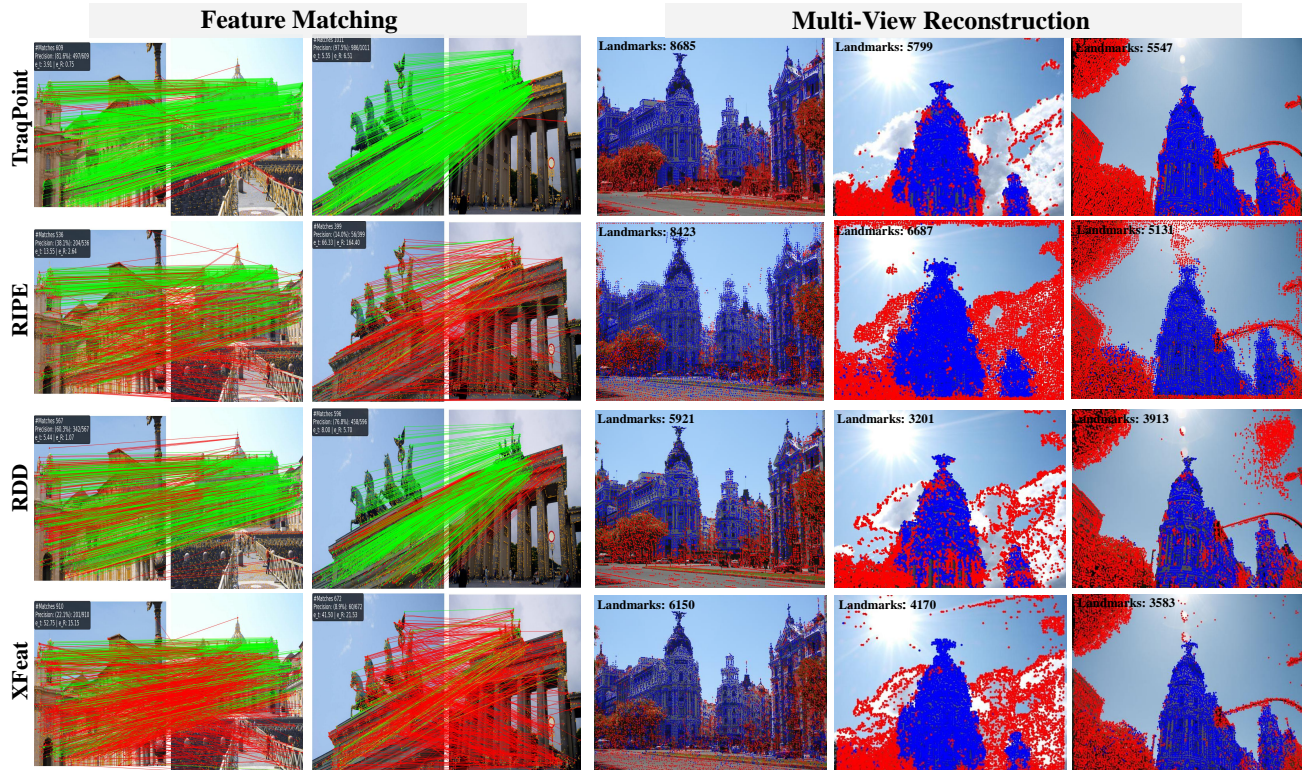


Figure 4. Qualitative results on the MegaDepth dataset [23] and the ETH benchmark [44]. For feature matching, keypoints are plotted in orange. Green lines indicate correct matches, while red lines denote incorrect ones. For multi-view reconstruction, keypoints that successfully generate point cloud landmarks are marked in blue; failed ones are marked in red. Our TraqPoint produces keypoints with better structural saliency and high cross-view consistency, which effectively improves feature matching and reconstruction tasks.

Table 1. Comparison on the MegaDepth [23] and ScanNet [8]. Top 4,096 features are used for all sparse matching methods. Best in bold, second best underlined.

Method	MegaDepth-1500			ScanNet		
	@5°	AUC ↑ @10°	@20°	@5°	AUC ↑ @10°	@20°
<i>Sparse with Learned Matcher</i>						
SP [9]+SG [40] CVPR'19	49.7	67.1	80.6	16.1	33.4	50.2
SP [9]+LG [24] ICCV'23	49.9	67.0	80.1	16.2	33.0	49.7
<i>Sparse with MNN</i>						
SuperPoint [9] CVPRW'18	24.1	40.0	54.7	7.0	17.2	29.8
DISK [48] NeurIPS'20	38.5	53.7	66.6	8.2	18.3	30.7
ALIKED [55] TMM'23	41.8	56.8	69.6	9.7	22.0	37.1
XFeat [33] CVPR'24	29.6	45.8	60.4	6.9	16.7	30.4
DeDoDe-V2-G [11] CVPRW'24	49.7	66.6	79.4	13.2	27.7	43.7
RDD [5] CVPR'25	<u>51.9</u>	<u>68.0</u>	<u>79.9</u>	<u>13.7</u>	<u>29.3</u>	<u>45.3</u>
RIPE [19] ICCV'25	45.4	60.8	72.9	9.4	20.5	33.5
TraqPoint (Ours)	<b>55.8</b>	<b>71.3</b>	<b>83.0</b>	<b>16.6</b>	<b>32.8</b>	<b>49.5</b>

2.9 on MegaDepth and ScanNet, respectively. We also gain significant matching accuracy advantages over RL-based methods including DISK [48] and RIPE [19]. Even with only the MNN matcher, our method delivers a 5.9 boost in AUC@5 boost on MegaDepth compared to methods equipped with extra matchers (e.g., SP+LG [24]), and achieves comparable accuracy on ScanNet—notably, our model is never trained on indoor data. As shown in Fig. 4, our method generates more structurally salient keypoints in

Table 2. Visual Localization on Aachen day-night [41]. Best in bold, second best underlined.

Methods	Day	Night
	(0.25m,2°) / (0.5m,5°) / (1.0m,10°)	
SuperPoint [9] CVPRW'18	87.4 / 93.2 / 97.0	77.6 / 85.7 / 95.9
DISK [48] NeurIPS'20	86.9 / <b>95.1</b> / 97.8	83.7 / 89.8 / 99.0
ALIKE [54] TMM'22	85.7 / 92.4 / 96.7	81.6 / 88.8 / <u>99.0</u>
ALIKED [55] TMM'23	86.5 / 93.4 / 96.8	<u>85.7</u> / 91.8 / 96.9
XFeat [33] CVPR'24	84.7 / 91.5 / 96.5	77.6 / 89.8 / 98.0
RDD [5] CVPR'25	87.0 / 94.2 / 97.8	<b>86.7</b> / <b>92.9</b> / 99.0
TraqPoint (Ours)	<b>87.9</b> / <b>95.1</b> / <b>97.9</b>	<u>85.7</u> / <b>92.9</b> / <b>100.0</b>

texture-rich regions with strong consistency even under extreme viewpoint variations, which further boosts the accuracy of pairwise matching.

#### 4.4. Visual Localization

**Dataset.** We validate TraqPoint’s performance on visual localization using the Aachen Day-Night dataset [41]. This dataset is specifically designed to localize high-quality nighttime images against a daytime 3D model, and it comprises 14,607 images covering variations in weather, season, viewpoint, and day-night cycles.

**Metrics and Compared Methods.** Following [5, 33], we use HLoc [39] to evaluate all methods [5, 9, 33, 48, 55].

Table 3. **Visual Odometry test results on sequence (01-03) of KITTI [14]**. ATE: Average Trajectory Error; MTE: Maximum Trajectory Error; AKTL: Average Keypoint Tracking Length.

Methods	ATE ↓	MTE ↓	AKTL ↑
<b>Seq-01</b>			
RootSIFT [1] <small>CVPR'12</small>	60.4	102.1	4.4
XFeat [33] <small>CVPR'24</small>	55.0	92.7	3.9
RDD [5] <small>CVPR'25</small>	<u>35.3</u>	<u>78.3</u>	<u>4.6</u>
RIPE [19] <small>ICCV'25</small>	43.7	90.6	4.1
TraqPoint (Ours)	<b>29.9</b>	<b>51.4</b>	<b>7.3</b>
<b>Seq-02</b>			
RootSIFT [1] <small>CVPR'12</small>	24.6	45.9	2.0
XFeat [33] <small>CVPR'24</small>	36.5	87.4	1.8
RDD [5] <small>CVPR'25</small>	<u>12.8</u>	<u>40.3</u>	<u>2.4</u>
RIPE [19] <small>ICCV'25</small>	35.4	82.3	1.7
TraqPoint (Ours)	<b>11.8</b>	<b>22.1</b>	<b>3.8</b>
<b>Seq-03</b>			
RootSIFT [1] <small>CVPR'12</small>	5.8	16.6	4.8
XFeat [33] <small>CVPR'24</small>	11.7	26.8	4.2
RDD [5] <small>CVPR'25</small>	4.0	11.2	<u>5.2</u>
RIPE [19] <small>ICCV'25</small>	<u>3.9</u>	<u>9.4</u>	4.8
TraqPoint (Ours)	<b>1.3</b>	<b>2.9</b>	<b>8.7</b>

Images are resized to a maximum side length of 1,024 pixels, and we sample the top 4,096 keypoints for all approaches. Metrics are computed using the evaluation tool from [41], including the AUC of estimated camera poses under threshold of  $\{0.25\text{m}, 0.5\text{m}, 1.0\text{m}\}$  for translation errors and  $\{2^\circ, 5^\circ, 10^\circ\}$  for rotation errors respectively.

**Results.** Tab. 2 presents the results of visual localization. TraqPoint achieves the best performance across all daytime settings and the two nighttime settings, further demonstrating its robustness.

#### 4.5. Visual Odometry (VO)

**Dataset.** Visual Odometry (VO) is a core component of SLAM systems, serving as a direct testbed for long-term keypoint trackability. We thus evaluate TraqPoint on the KITTI Odometry Benchmark [14], which provides 22 stereo image sequences covering diverse real-world driving scenarios (e.g., varying illumination, dynamic objects). Among these sequences, 10 are accompanied by ground-truth trajectories annotated via high-precision GPS/IMU for quantitative evaluation. We report the results of sequences 01–03, while the results of the remaining sequences along with detailed definitions of the metrics are included in the supplementary material.

**Metrics and Compared Methods.** We evaluate odometry benchmark from two perspectives: trajectory estimation accuracy and keypoint tracking consistency. For trajectory accuracy, we compute Average Trajectory Error (ATE) and Maximum Trajectory Error (MTE) by calculating 2D positional errors of projected  $x$ - $z$  plane trajectories. For keypoint tracking consistency, Average Keypoint Tracking Length (AKTL) is defined as the mean tracking length of valid keypoints. We compared TraqPoint against the hand-crafted features [1] and learnable detectors [5, 19, 33]. All

Table 4. **Results on ETH benchmark [44] for 3D reconstruction.** Best in bold, second best underlined.

Methods	Reg. Img↑	Sparse Pts↑	Track Len↑	Reproj Err↓
<b>Madrid Metropolis (1344 imgs)</b>				
RootSIFT [1] <small>CVPR'12</small>	500	116k	6.32	<b>0.60px</b>
SuperPoint [9] <small>CVPRW'18</small>	438	29k	9.03	1.05px
D2-Net [10] <small>CVPR'19</small>	501	84k	6.33	1.28px
ASLFeat [27] <small>CVPR'20</small>	613	96k	8.76	0.90px
PosFeat [22] <small>CVPR'22</small>	419	72k	9.18	<u>0.86px</u>
XFeat [33] <small>CVPR'24</small>	581	111k	6.16	1.27px
RDD [5] <small>CVPR'25</small>	632	154k	<u>9.40</u>	1.12px
RIPE [19] <small>ICCV'25</small>	<u>644</u>	<u>167k</u>	5.87	1.25px
TraqPoint (Ours)	<b>693</b>	<b>254k</b>	<b>11.14</b>	1.03px
<b>Gendarmen-markt (1463 imgs)</b>				
RootSIFT [1] <small>CVPR'12</small>	1035	<u>338k</u>	5.52	<b>0.69px</b>
SuperPoint [9] <small>CVPRW'18</small>	967	93k	7.22	1.03px
D2-Net [10] <small>CVPR'19</small>	1053	250k	5.08	1.19px
ASLFeat [27] <small>CVPR'20</small>	1040	221k	8.72	1.00px
PosFeat [22] <small>CVPR'22</small>	956	240k	8.40	<u>0.92px</u>
XFeat [33] <small>CVPR'24</small>	1049	276k	6.74	1.30px
RDD [5] <small>CVPR'25</small>	1062	309k	<u>9.87</u>	1.17px
RIPE [19] <small>ICCV'25</small>	<u>1069</u>	321k	7.21	1.26px
TraqPoint (Ours)	<b>1093</b>	<b>401k</b>	<b>11.06</b>	1.08px
<b>Tower of London (1576 imgs)</b>				
RootSIFT [1] <small>CVPR'12</small>	804	239k	7.76	<b>0.61px</b>
SuperPoint [9] <small>CVPRW'18</small>	681	52k	8.67	0.96px
D2-Net [10] <small>CVPR'19</small>	785	180k	5.32	1.24px
ASLFeat [27] <small>CVPR'20</small>	821	222k	12.16	0.92px
PosFeat [22] <small>CVPR'22</small>	778	262k	11.64	<u>0.90px</u>
XFeat [33] <small>CVPR'24</small>	796	244k	8.50	1.28px
RDD [5] <small>CVPR'25</small>	<u>834</u>	<u>278k</u>	<u>12.20</u>	1.15px
RIPE [19] <small>ICCV'25</small>	823	269k	9.14	1.25px
TraqPoint (Ours)	<b>875</b>	<b>341k</b>	<b>13.28</b>	1.06px

methods use the top-4096 keypoints for prediction, and adopt mutual nearest neighbor (MNN) matching.

**Results.** Tab. 3 presents our performance on the odometry task. Our method achieves the best results in both Average Trajectory Error and Maximum Trajectory Error. Notably, it delivers remarkable gains in the Average Keypoint Trajectory Length (AKTL) metric—outperforming RDD [5] and RIPE [19] with significant margins. Even under outdoor fast-motion and associated challenges (rapid texture changes, dynamic objects), our keypoints still maintain good spatial consistency in temporal sequences, enabling more stable camera pose and trajectory estimation.

#### 4.6. 3D Reconstruction

**Dataset.** We use the ETH benchmark [44] to demonstrate effectiveness on 3D reconstruction tasks. Following prior works [22, 27], we evaluate on three medium-scale scenes from this benchmark.

**Metrics and Compared Methods.** For each scene, we perform matching with a ratio test of 0.8 and mutual check for outlier rejection, followed by SfM algorithm execution using COLMAP [43]. We then report the number of registered images (Reg. Images), the number of sparse points (Sparse Pts), average track length (Track Len) and mean re-

Table 5. Ablation study. We report matching capability (AUC@5° on MegaDepth [23]) and tracking stability (average value of AKTL on KITTI [14] sequence 01-03).

Variant	AUC@5° ↑	AKTL ↑
<b>TraqPoint-Full (Ours)</b>	<b>55.8</b>	<b>6.6</b>
<i>1. RL Paradigm</i>		
TraqPoint – Pairwise	53.3	4.3
Match Reward – Pairwise	49.7	2.8
<i>2. Reward Function Design</i>		
w/o Ranking Reward	52.6	4.0
w/o Distinctiveness Reward	54.6	5.9
w/o RL learning	52.0	3.8
<i>3. Backbone Architecture</i>		
DINOv2-ViT	54.8	6.4
ResNet-50	54.5	6.1

projection error (Reproj. Error). The maximum number of keypoints is limited to 20k for all methods.

**Results.** Tab. 4 demonstrates the effectiveness of our method in multi-view sparse reconstruction. Our approach achieves the best performance across key metrics: the number of registered images, generated point cloud number, and keypoint track length. The marginal increase in reprojection error stems from retaining “hard” keypoints (*e.g.*, under large viewpoint changes), which are essential for the significant gains in reconstruction density and track length. These results reflect that the strong consistency of our keypoints effectively boosts reconstruction quality. Further visualizations in Fig. 4 demonstrate that our keypoints yield a more rational distribution: they are less likely to fall into texture-less regions (*e.g.*, sky) and instead exhibit a more regular, structured arrangement in texture-rich areas. This favorable spatial consistency directly contributes to improved performance in the reconstruction task.

#### 4.7. Ablation

We report two metrics: AUC@5 on the MegaDepth dataset [23], measuring matching capability. The AKTL metric on KITTI sequences 01–03 [14], directly quantifying keypoint consistency. Results are shown in Tab. 5:

**1) Sequential vs. Pairwise Reinforcement Learning.** Two variants are constructed: (i) a two-frame simplified version, where rewards are computed solely on single image pairs to back propagate and optimize the policy network; (ii) using a basic matching reward (award keypoints form nearest-neighbor matches with projected points), consistent with pairwise matching reward designs in most RL frameworks [19, 48]. Results show sequentialization improves AUC@5 by 2.5 and AKTL by 2.3. Additionally, our custom reward outperforms the basic match reward.

**2) Reward Function Design.** We ablate our two reward components against a baseline of RDD-based supervised training (without RL). Results show that the ranking reward yields substantial performance gains by enforc-

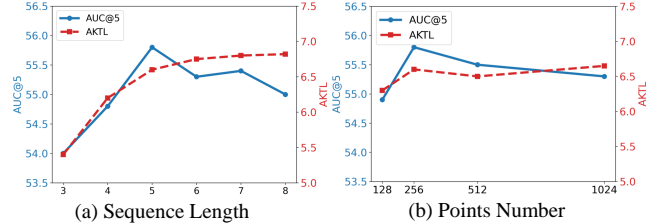


Figure 5. Ablation study on sequence length and the number of sampled keypoints.

ing keypoint repeatability. The distinctiveness reward further elevates keypoint distinctiveness, effectively mitigating false matches. The supervised baseline exhibits marked performance degradation, underscoring the indispensable role of our RL framework in optimizing long-term trackability.

**3) Backbone Architecture Analysis.** Existing work confirms pre-trained backbones boost descriptor robustness [5, 11, 17]. We evaluate two representatives: ResNet-50 [16] and DINOv2-ViT [30], where DINOv2-ViT only shows marginal gains over ResNet-50—we attribute this to its lack of multi-scale feature representation capabilities. Thus, we adopt DINOv3-ConvNeXt in experiments, as it possesses both multi-scale features and strong semantic representation abilities. Notably, our sequence-aware RL yields consistent gains across all backbones, indicating the paradigm complements (not merely relies on) descriptor quality.

**4) Hyperparameter Sensitivity.** We investigate two key hyperparameters: training sequence length and number of sampled keypoints. For sequence length, increasing it enhances reward stability, but an excessively long sequence diminishes the average effective information. As shown in Fig. 5, the optimal parameters are a training sequence length of 5 and 256 sampled keypoints.

## 5. Conclusion

In this paper, we present a novel sequence-aware paradigm for learning local keypoints. We identify a critical gap in previous methods—the reliance on pairwise matching objective that optimizes for short-term matchability rather than long-term consistency. To address this gap, we reformulate keypoint detection as a sequential decision-making problem and introduce a reinforcement learning framework trained with a novel composite reward that jointly enhances multi-view consistency and distinctiveness. Extensive experiments demonstrate that our approach outperforms existing methods across both pairwise and sequence-based downstream tasks. Thus, our work offers a novel research perspective for boosting the long-term stability of keypoints in sequential vision systems.

**Acknowledgment.** This work was supported partially by the National Key Research and Development Program of China (2023YFC2705700), NSFC 62222112, 62176186, and the NSF of Hubei Province of China (2024AFB245).

## References

- [1] Relja Arandjelović and Andrew Zisserman. Three things everyone should know to improve object retrieval. In *Proc. IEEE/CVF Conf. Comput. Vis. Pattern Recog.*, pages 2911–2918, 2012. 7
- [2] Giovanni Barbarani, Francesco Vaccarino, Gabriele Trivigno, Marco Guerra, Gabriele Berton, and Carlo Masone. Scale-free image keypoints using differentiable persistent homology. In *Proc. Int. Conf. Mach. Learn.*, pages 2990–3002, 2024. 2
- [3] Aritra Bhowmik, Stefan Gumhold, Carsten Rother, and Eric Brachmann. Reinforced feature points: Optimizing feature detection and description for a high-level task. In *Proc. IEEE/CVF Conf. Comput. Vis. Pattern Recog.*, pages 4948–4957, 2020. 1, 2
- [4] Gary Bradski. The OpenCV library. *Dr. Dobbs's Journal: Software Tools for the Professional Programmer*, 25(11): 120–123, 2000. 5
- [5] Gonglin Chen, Tianwen Fu, Haiwei Chen, Wenbin Teng, Hanyuan Xiao, and Yajie Zhao. RDD: Robust feature detector and descriptor using deformable transformer. In *Proc. IEEE/CVF Conf. Comput. Vis. Pattern Recog.*, pages 6394–6403, 2025. 1, 2, 3, 5, 6, 7, 8
- [6] Chi-Ming Chung, Yang-Che Tseng, Ya-Ching Hsu, Xiang-Qian Shi, Yun-Hung Hua, Jia-Fong Yeh, Wen-Chin Chen, Yi-Ting Chen, and Winston H Hsu. Orbeez-SLAM: A real-time monocular visual slam with orb features and nerf-realized mapping. In *Proc. IEEE Int. Conf. Robot. Autom.*, pages 9400–9406, 2023. 1
- [7] Titus Cieslewski, Konstantinos G Derpanis, and Davide Scaramuzza. SIPs: Succinct interest points from unsupervised inlier probability learning. In *International Conference on 3D Vision*, pages 604–613, 2019. 2
- [8] Angela Dai, Angel X Chang, Manolis Savva, Maciej Halber, Thomas Funkhouser, and Matthias Nießner. ScanNet: Richly-annotated 3D reconstructions of indoor scenes. In *Proc. IEEE/CVF Conf. Comput. Vis. Pattern Recog.*, pages 5828–5839, 2017. 5, 6
- [9] Daniel DeTone, Tomasz Malisiewicz, and Andrew Rabinovich. SuperPoint: Self-supervised interest point detection and description. In *Proc. of IEEE Conf. Comput. Vis. Pattern Recognit. Workshops*, pages 224–236, 2018. 1, 2, 5, 6, 7
- [10] Mihai Dusmanu, Ignacio Rocco, Tomas Pajdla, Marc Pollefeys, Josef Sivic, Akihiko Torii, and Torsten Sattler. D2-Net: A trainable cnn for joint description and detection of local features. In *Proc. IEEE/CVF Conf. Comput. Vis. Pattern Recog.*, pages 8092–8101, 2019. 2, 7
- [11] Johan Edstedt, Georg Bökman, and Zhenjun Zhao. DeDoDe v2: Analyzing and Improving the DeDoDe Keypoint Detector. In *Proc. of IEEE Conf. Comput. Vis. Pattern Recognit. Workshops*, 2024. 1, 2, 3, 5, 6, 8
- [12] Johan Edstedt, Qiyu Sun, Georg Bökman, Mårten Wadenbäck, and Michael Felsberg. RoMa: Robust dense feature matching. In *Proc. IEEE/CVF Conf. Comput. Vis. Pattern Recog.*, pages 19790–19800, 2024. 2
- [13] Johan Edstedt, Georg Bökman, Mårten Wadenbäck, and Michael Felsberg. DaD: Distilled reinforcement learning for diverse keypoint detection. *arXiv preprint arXiv:2503.07347*, 2025. 2
- [14] Andreas Geiger, Philip Lenz, and Raquel Urtasun. Are we ready for autonomous driving? the KITTI vision benchmark suite. In *Proc. IEEE/CVF Conf. Comput. Vis. Pattern Recog.*, pages 3354–3361, 2012. 7, 8
- [15] Pierre Gleize, Weiyao Wang, and Matt Feiszli. SiLK: Simple learned keypoints. In *Proc. IEEE/CVF Int. Conf. Comput. Vis.*, pages 22499–22508, 2023. 1, 2
- [16] Kaiming He, Xiangyu Zhang, Shaoqing Ren, and Jian Sun. Deep residual learning for image recognition. In *Proc. IEEE/CVF Conf. Comput. Vis. Pattern Recog.*, pages 770–778, 2016. 8
- [17] Hanwen Jiang, Arjun Karapur, Bingyi Cao, Qixing Huang, and Andre Araujo. OmniGlue: Generalizable feature matching with foundation model guidance. In *Proc. IEEE/CVF Conf. Comput. Vis. Pattern Recog.*, 2024. 8
- [18] Shinjeong Kim, Marc Pollefeys, and Daniel Barath. Learning to make keypoints sub-pixel accurate. In *Proc. Eur. Conf. Comput. Vis.*, pages 413–431, 2024. 2
- [19] Johannes Künzel, Anna Hilsmann, and Peter Eisert. RIPE: Reinforcement learning on unlabeled image pairs for robust keypoint extraction. In *Proc. IEEE/CVF Int. Conf. Comput. Vis.*, 2025. 1, 2, 5, 6, 7, 8
- [20] Jongmin Lee, Byungjin Kim, and Minsu Cho. Self-supervised equivariant learning for oriented keypoint detection. In *Proc. IEEE/CVF Conf. Comput. Vis. Pattern Recog.*, pages 4847–4857, 2022. 2
- [21] Vincent Leroy, Yohann Cabon, and Jérôme Revaud. Grounding image matching in 3d with MAST3R. In *Proc. Eur. Conf. Comput. Vis.*, pages 71–91, 2024. 2
- [22] Kunhong Li, Longguang Wang, Li Liu, Qing Ran, Kai Xu, and Yulan Guo. Decoupling makes weakly supervised local feature better. In *Proc. IEEE/CVF Conf. Comput. Vis. Pattern Recog.*, pages 15838–15848, 2022. 7
- [23] Zhengqi Li and Noah Snavely. MegaDepth: Learning single-view depth prediction from internet photos. In *Proc. IEEE/CVF Conf. Comput. Vis. Pattern Recog.*, pages 2041–2050, 2018. 1, 2, 3, 5, 6, 8
- [24] Philipp Lindenberger, Paul-Edouard Sarlin, and Marc Pollefeys. LightGlue: Local feature matching at light speed. In *Proc. IEEE/CVF Int. Conf. Comput. Vis.*, pages 17627–17638, 2023. 5, 6
- [25] Yepeng Liu, Wenpeng Lai, Zhou Zhao, Yuxuan Xiong, Jinchu Zhu, Jun Cheng, and Yongchao Xu. LiftFeat: 3D geometry-aware local feature matching. In *Proc. IEEE Int. Conf. Robot. Autom.*, pages 11714–11720, 2025. 1
- [26] David G Lowe. Distinctive image features from scale-invariant keypoints. *Int. J. Comput. Vis.*, 60:91–110, 2004. 2, 5
- [27] Zixin Luo, Lei Zhou, Xuyang Bai, Hongkai Chen, Jiahui Zhang, Yao Yao, Shiwei Li, Tian Fang, and Long Quan. ASLFeat: Learning local features of accurate shape and localization. In *Proc. IEEE/CVF Conf. Comput. Vis. Pattern Recog.*, pages 6589–6598, 2020. 7
- [28] Jiri Matas, Ondrej Chum, Martin Urban, and Tomás Pajdla. Robust wide-baseline stereo from maximally stable ex-

- tremal regions. *Image and vision computing*, 22(10):761–767, 2004. 2
- [29] Raul Mur-Artal and Juan D Tardós. ORB-SLAM2: An open-source slam system for monocular, stereo, and RGB-D cameras. *IEEE Trans. Robot.*, 33(5):1255–1262, 2017. 1
- [30] Maxime Oquab, Timothée Darcet, Théo Moutakanni, Huy V Vo, Marc Szafraniec, Vasil Khalidov, Pierre Fernandez, Daniel HAZIZA, Francisco Massa, Alaaeldin El-Nouby, et al. DINOv2: Learning robust visual features without supervision. *Transactions on Machine Learning Research*, 2024. 8
- [31] Konstantin Pakulev, Alexander Vakhitov, and Gonzalo Ferrer. Ness-st: Detecting good and stable keypoints with a neural stability score and the Shi-Tomasi detector. In *Proc. IEEE/CVF Int. Conf. Comput. Vis.*, pages 9578–9588, 2023. 2
- [32] Guilherme Potje, Felipe Cadar, André Araujo, Renato Martins, and Erickson R Nascimento. Enhancing deformable local features by jointly learning to detect and describe keypoints. In *Proc. IEEE/CVF Conf. Comput. Vis. Pattern Recog.*, pages 1306–1315, 2023. 2
- [33] Guilherme Potje, Felipe Cadar, André Araujo, Renato Martins, and Erickson R Nascimento. XFeat: Accelerated features for lightweight image matching. In *Proc. IEEE/CVF Conf. Comput. Vis. Pattern Recog.*, pages 2682–2691, 2024. 2, 3, 5, 6, 7
- [34] Jerome Revaud, Cesar De Souza, Martin Humenberger, and Philippe Weinzaepfel. R2D2: Reliable and repeatable detector and descriptor. *Adv. Neural Inf. Process. Syst.*, 32, 2019. 2
- [35] Edward Rosten, Reid Porter, and Tom Drummond. Faster and better: A machine learning approach to corner detection. *IEEE Trans. on Pattern Anal. and Mach. Intell.*, 32(1):105–119, 2008. 2, 5
- [36] Ethan Rublee, Vincent Rabaud, Kurt Konolige, and Gary Bradski. ORB: An efficient alternative to SIFT or SURF. In *Proc. IEEE/CVF Int. Conf. Comput. Vis.*, pages 2564–2571, 2011. 2
- [37] Emanuele Santellani, Christian Sormann, Mattia Rossi, Andreas Kuhn, and Friedrich Fraundorfer. S-TREK: Sequential translation and rotation equivariant keypoints for local feature extraction. In *Proc. IEEE/CVF Int. Conf. Comput. Vis.*, pages 9728–9737, 2023. 2
- [38] Emanuele Santellani, Martin Zach, Christian Sormann, Mattia Rossi, Andreas Kuhn, and Friedrich Fraundorfer. Gmm-ikrs: Gaussian mixture models for interpretable keypoint refinement and scoring. In *Proc. Eur. Conf. Comput. Vis.*, pages 77–93, 2024. 2
- [39] Paul-Edouard Sarlin, Cesar Cadena, Roland Siegwart, and Marcin Dymczyk. From coarse to fine: Robust hierarchical localization at large scale. In *Proc. IEEE/CVF Conf. Comput. Vis. Pattern Recog.*, pages 12716–12725, 2019. 1, 6
- [40] Paul-Edouard Sarlin, Daniel DeTone, Tomasz Malisiewicz, and Andrew Rabinovich. SuperGlue: Learning feature matching with graph neural networks. In *Proc. IEEE/CVF Conf. Comput. Vis. Pattern Recog.*, pages 4938–4947, 2020. 5, 6
- [41] Torsten Sattler, Will Maddern, Carl Toft, Akihiko Torii, Lars Hammarstrand, Erik Stenborg, Daniel Safari, Masatoshi Okutomi, Marc Pollefeys, Josef Sivic, et al. Benchmarking 6DOF outdoor visual localization in changing conditions. In *Proc. IEEE/CVF Conf. Comput. Vis. Pattern Recog.*, pages 8601–8610, 2018. 6, 7
- [42] Nikolay Savinov, Akihito Seki, Lubor Ladicky, Torsten Sattler, and Marc Pollefeys. Quad-networks: unsupervised learning to rank for interest point detection. In *Proc. IEEE/CVF Conf. Comput. Vis. Pattern Recog.*, pages 1822–1830, 2017. 2
- [43] Johannes L Schonberger and Jan-Michael Frahm. Structure-from-motion revisited. In *Proc. IEEE/CVF Conf. Comput. Vis. Pattern Recog.*, pages 4104–4113, 2016. 1, 2, 7
- [44] Johannes L Schonberger, Hans Hardmeier, Torsten Sattler, and Marc Pollefeys. Comparative evaluation of hand-crafted and learned local features. In *Proc. IEEE/CVF Conf. Comput. Vis. Pattern Recog.*, pages 1482–1491, 2017. 6, 7
- [45] Oriane Siméoni, Huy V. Vo, Maximilian Seitzer, Federico Baldassarre, Maxime Oquab, Cijo Jose, Vasil Khalidov, Marc Szafraniec, Seungeun Yi, Michaël Ramamonjisoa, Francisco Massa, Daniel Haziza, Luca Wehrstedt, Jianyuan Wang, Timothée Darcet, Théo Moutakanni, Leonel Sentana, Claire Roberts, Andrea Vedaldi, Jamie Tolan, John Brandt, Camille Couprie, Julien Mairal, Hervé Jégou, Patrick Labatut, and Piotr Bojanowski. DINOv3, 2025. 3
- [46] Jiaming Sun, Zehong Shen, Yuang Wang, Hujun Bao, and Xiaowei Zhou. LoFTR: Detector-free local feature matching with transformers. In *Proc. IEEE/CVF Conf. Comput. Vis. Pattern Recog.*, pages 8922–8931, 2021. 2
- [47] Prune Truong, Stefanos Apostolopoulos, Agata Mosinska, Samuel Stucky, Carlos Ciller, and Sandro De Zanet. GLAMPoints: Greedily learned accurate match points. In *Proc. IEEE/CVF Int. Conf. Comput. Vis.*, pages 10732–10741, 2019. 2
- [48] Michał Tyszkiewicz, Pascal Fua, and Eduard Trulls. DISK: Learning local features with policy gradient. *Adv. Neural Inf. Process. Syst.*, 33:14254–14265, 2020. 1, 2, 5, 6, 8
- [49] Shuzhe Wang, Vincent Leroy, Yohann Cabon, Boris Chidlovskii, and Jerome Revaud. DUST3R: Geometric 3D vision made easy. In *Proc. IEEE/CVF Conf. Comput. Vis. Pattern Recog.*, pages 20697–20709, 2024. 2
- [50] Xinjiang Wang, Zeyu Liu, yu Hu, Wei Xi, Wenxian Yu, and Danping Zou. FeatureBooster: Boosting feature descriptors with a lightweight neural network. In *Proc. IEEE/CVF Conf. Comput. Vis. Pattern Recog.*, 2023. 1
- [51] Yifan Wang, Xingyi He, Sida Peng, Dongli Tan, and Xiaowei Zhou. Efficient LoFTR: Semi-dense local feature matching with sparse-like speed. In *Proc. IEEE/CVF Conf. Comput. Vis. Pattern Recog.*, pages 21666–21675, 2024. 2
- [52] Yongchao Xu, Pascal Monasse, Thierry Géraud, and Laurent Najman. Tree-based morse regions: A topological approach to local feature detection. *IEEE Trans. Image Process.*, 23(12):5612–5625, 2014. 2
- [53] Peng Yin, Ivan Cisneros, Shiqi Zhao, Ji Zhang, Howie Choset, and Sebastian Scherer. iSimLoc: Visual global localization for previously unseen environments with simulated images. *IEEE Trans. Robot.*, 39(3):1893–1909, 2023. 1

- [54] Xiaoming Zhao, Xingming Wu, Jinyu Miao, Weihai Chen, Peter CY Chen, and Zhengguo Li. ALIKE: Accurate and lightweight keypoint detection and descriptor extraction. *IEEE Trans. on Multimedia*, 25:3101–3112, 2022. [6](#)
- [55] Xiaoming Zhao, Xingming Wu, Weihai Chen, Peter CY Chen, Qingsong Xu, and Zhengguo Li. ALIKED: A lighter keypoint and descriptor extraction network via deformable transformation. *IEEE Trans. Instrum. Meas.*, 72:1–16, 2023. [1](#), [2](#), [3](#), [5](#), [6](#)